Available online at www.sciencedirect.com

Manufacturing Letters

Manufacturing Letters 44 (2025) 1306–1315

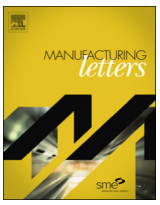

53rd SME North American Manufacturing Research Conference (NAMRC 53, 2025)

Automating Transfer Function Estimation: LSRF Method with Coherence-Based Pre-Filtering and Weighting Filters

Florian Oexle[a,*], Fabian Heimberger[a], Alexander Puchta[a], Jürgen Fleischer[a]

[a]*wbk Institute of Production Science, Karlsruhe Institute of Technology (KIT), Kaiserstraße 12, 76131 Karlsruhe, Germany*

Abstract

The increasing individualization of products, coupled with a shortage of skilled workers in the fields of science, technology, engineering and mathematics (STEM), is a challenge for manufacturing companies worldwide. To achieve batch size 1 production without the expertise of longtime employees, machine tools must be able to automatically optimize machining processes in virtual space prior to execution. This requires simulation of the machining process. Therefore digital models are needed that represent machine tool and process behavior. However, due to a lack of skilled workers, these models must be built by the machine tools themselves. Based on a previous publication by Oexle et al., this paper presents a methodology for automating transfer function estimation using the least squares rational function (LSRF) method combined with coherence-based pre-filtering and the use of specific weighting filters. Fits >70 % could be achieved on measurement data sets with good coherence. However, for measurement data sets with poor coherence, good fits are possible but not guaranteed.

Peer-review under responsibility of the scientific committee of the NAMRI/SME.

Keywords: Modelling; Simulation; Digital Twin; Machine Tool

1. Introduction

Increasing product individualization and a persistent shortage of skilled workers in the fields of science, technology, engineering and mathematics (STEM) are two of the biggest challenges facing manufacturing today [34, 21, 9]. Both challenges influence each other. The increasing individualization of products requires batch size 1 production [16]. However, this can only be realized with the help of skilled workers. Within the framework of Industry 4.0, it is possible to simulate both process and machine behavior to enable automated optimization of the real process upstream of the production process, making it possible to realize batch size 1 production without skilled workers [16]. As a result, all specified tolerances can be met in real production from part 1. This significantly reduces the need for skilled workers and the reject rate of the produced components. A central component for the simulation of such process and machine behavior are the Digital Twin and Digital Shadow [5, 4]. However, building the contained digital models needed to perform the above-mentioned simulations is currently being done manually [14]. This approach is both time-consuming and dependent on expert knowledge. In order to avoid the resulting need to shift skilled workers from the use of machines to the modeling of process and machine behavior, the digital models contained in the Digital Twin and Digital Shadow must be built automatically in the future. For this purpose, a concept has already been presented by Oexle et al. that allows a milling machine to automatically build a model of its own machine-dynamic behavior individually and keep it up-to-date over its entire lifetime [19]. Figure 1 provides an overview of the approach presented by Oexle et al. The machine tool's dynamic behavior is modeled based on linear time-invariant (LTI) systems that map autonomously measured compliance frequency response functions (FRFs) at discrete spatial points in the machine's working area. Each of these FRF contains the transmission behavior from a force excitation at the tool tip to the resulting displacement at the spindle nose. The a priori LTI model is

* Corresponding author. Tel.: +49-174-330-2745 ; fax: +49-721-608-45005.
E-mail address: florian.oexle@kit.edu (Florian Oexle).

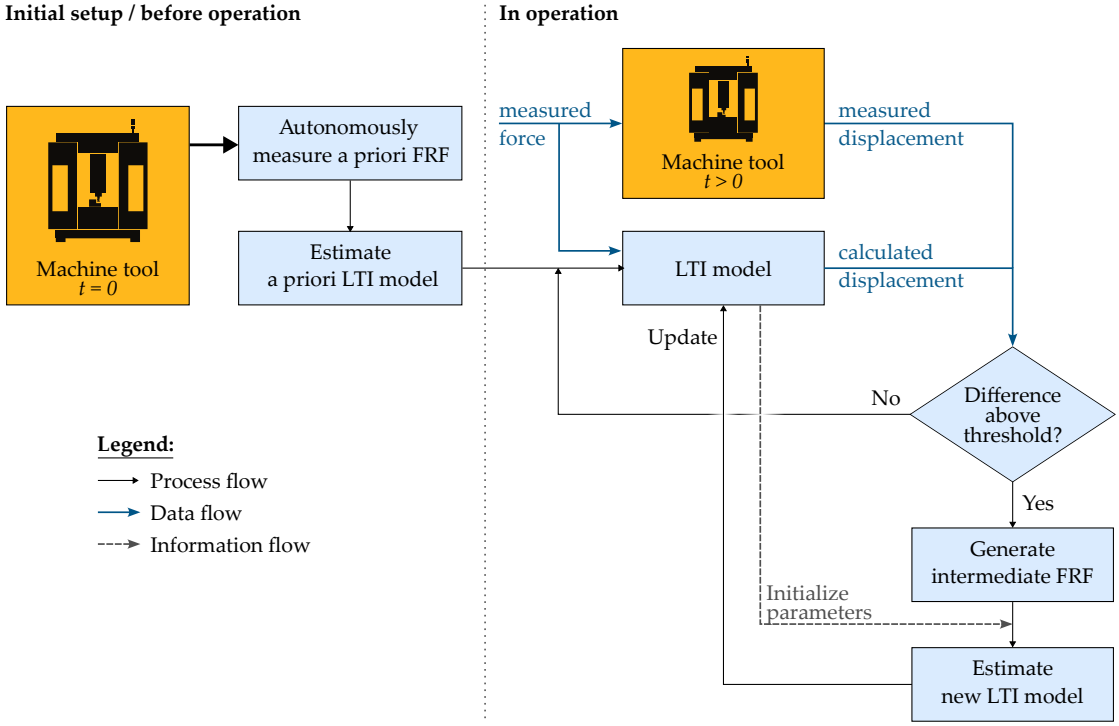

Figure 1. Methodology presented by Oexle et al. [19] for modeling the individual and lifetime-adaptive dynamic behavior of machine tools. The initial setup of the machine tool's a priori LTI models is performed at $t = 0$ (left side). During the machine tool's lifetime $t > 0$, its dynamic behavior changes and the update procedure is conducted (right side). The scope of this paper is the estimation of a priori LTI model.

built at time $t = 0$ (Figure 1, left side). During part production, the machine records both the force acting on the spindle and the resulting displacement at the level of the spindle nose (Figure 1, right side). The displacement of the spindle nose can then be simulated using the measured force and the estimated a priori LTI model. It is then compared to the actual measured displacement. If significant differences are found between the two displacement time series, the model is assumed to contain an error. In this case, the model is updated based on measured data collected during normal machine operation. This concept has been tested and validated using noise-free synthetic data obtained from simulation [19].

The aim of this paper is to examine the practical implementation of the concept using actual measurement data. In particular, the setup of the a priori LTI model (Figure 1, left side) is considered. This paper demonstrates the methodology for the automatic construction of a LTI model in the form of a transfer function based on a measured FRF.

This paper is structured as follows: Chapter 2 discusses the current state of the art in modal parameter identification and mathematical modeling of system behavior in general. This is followed by Chapter 3, which presents the authors' own methodology based on the least squares rational function (LSRF) method (implemented in Matlab's `tfest` command) combined with various pre-filtering using the coherence of the measured FRFs and the usage of specific weighting filters. Chapter 4 concludes with a brief summary and outlook for further work.

Nomenclature

$D(s)$	denominator polynomial of $G(s)$
$G(s)$	estimated time-continuous transfer function
$H(j\omega_i)$	measured compliance frequency response function at $i = 1 \dots N_f$ sampled frequency points
J	cost function
k	timestep
$N(s)$	numerator polynomial of $G(s)$
u	measured or simulated force force
$W(j\omega_i)$	weighting filter
$\hat{y}$	simulated displacement
γ^2	coherence

Abbreviations

FRAC	frequency response assurance criterion
FRF	compliance frequency response function
LSRF	least squares rational function
LTI	linear time-invariant
MDOF	multi-degree-of-freedom
NRMSE	normalized root mean squared error
SDOF	single-degree-of-freedom
STEM	science, technology, engineering and mathematics

2. State of the Art

There are several methods to describe a FRF in a mathematical form. Typically, the description of modal models consisting of the modal parameters eigenfrequencies, mode shapes and modal damping is used because of its intuitive physical interpretability [31]. Depending on the complexity involved, they are estimated using one of two methods: the single-degree-of-freedom (SDOF) and the multi-degree-of-freedom (MDOF) methods [8]. The most widely used SDOF methods are peak-picking, circle-fit and line-fit methods [8]. In addition, the two-stage least squares identification by Altintas is known [1]. All of these methods have the goal of determining only a single mode of an FRF at a time, which requires a clear independence of its FRF behavior from other modes. If this condition is not met, MDOF methods are used [8]. The most well-known of these are the global rational fractional polynomial method [8], the LSRF method [2], the global singular value decomposition (SVD) method [8], the least squares complex exponential (LSCE) method [32], the domain least squares complex frequency (LSCF) method and its polyreference version, the so-called "PolyMAX" [11, 20] method, and various stochastic subspace identification (SSI) methods [30]. The PolyMAX method is particularly popular in the field of modal analysis due to its exceptionally good support for the identification of physical modes based on a stabilization diagram. However, all of these methods share a fundamental limitation: at a minimum, the model order, and thus the number of modes, must be specified to estimate the modal parameters. In some cases, additional hyperparameters must also be defined.

Numerous studies have already dealt with the automatic determination of these hyperparameters. Scionti et al. present a method to eliminate non-physical modes in two steps based on rules representing human mode selection [26]. Lau et al. extend this work by presenting a rule-based automatic modal parameter selection approach [15]. Based on validation experiments with two groups consisting of modal analysis experts and novices, it was found that an overall productivity gain of 50 % can be achieved independent of previous knowledge. At a later stage, Scionti and Lanslots considered various fuzzy c-means clustering techniques, some in combination with a genetic algorithm and some not, for finding pole candidates [25]. The result was evaluated as positive in comparison with the poles found manually by experts. Reyenders et al. were the first to present an approach that allows fully automated interpretation of stabilization diagrams and thus filtering out physical modes [23]. They set up a three-stage procedure for this purpose. In the first stage, all modes of a stabilization diagram are classified into two categories: possible physical modes and certainly spurious modes. This is done using as many relevant single mode validation criterias as possible. Modes classified as certainly spurious are removed directly from the stabilization diagram. The resulting cleaned diagram may still contain spurious modes, so the remaining modes are classified as possible physical modes. In the second stage, similar modes of the remaining modes are clustered together. Hierarchical clustering is used to find similar modes and group them accordingly. In the third stage, the clusters formed are again divided into the two categories of physical and spurious modes, and a single mode is derived from each cluster of physical modes. Neu et al. followed an approach similar to that of Reyender et al. [18]. However, they found that their approach was less sensitive than that of Reyender et al. Mugnaini et al. later extended the method of Neu et al. [17]. In the studies by Reyender et al., Neu et al. and Mugnaini et al. the modes found were only validated against manual mode selection by experts. There was no validation based on the final reproducibility of the measured FRF. On this basis, Ellinger et al. presented a method that does not evaluate the accuracy of the modal parameter estimation, but rather the mapping accuracy of the resulting modal model [7]. They used the frequency response assurance criterion (FRAC) [13] extended by a term to obtain the smallest possible number of modes. The estimation of the modal parameters for the subsequent construction of the modal model was performed using the PolyMAX algorithm combined with Bayesian optimization, which determined a total of eight hyperparameters. Compared to Matlab's `modalfit` function, similar and in some cases better mode identification could be achieved, while the computational time was significantly reduced.

3. Proposed methodology for estimating a transfer function

In summary, the current state of the art in FRF modeling is focused on the estimation of modal parameters. This is a reasonable approach, as it offers intuitive physical insights into the occurrence of vibrations at different frequencies and the respective components responsible for generating these vibrations [33]. According to the approach presented by Oexle et al., which focuses on displacement simulation, a mathematical description of the FRF is required instead of estimating the modal parameters [19]. After the estimation of this mathematical description, in a subsequent step, the displacement simulation is conducted at the spindle nose based on a time series of force measurements. In this context, the LSRF method implemented with the Matlab command `tfest` [29] is employed as a tool for estimating a transfer function, as described in detail by Ozdemir and Gumussoy [2]. The aim of `tfest` is to minimize the cost function

$$J = \min_{G(j\omega_i)} \sum_{i=1}^{N_f} \left| W(j\omega_i) \left[G(j\omega_i) - H(j\omega_i) \right] \right|^2 , \qquad (1)$$

where H represents the measured FRF and N_f the number of frequency points.

The algorithm has several advantages for the application of the given problem:

1. The result is a estimated time-continuous transfer function

$$G(s) = \frac{N(s)}{D(s)} = \frac{a_0 + a_1 s + \cdots + a_m s^m}{b_0 + b_1 s + \cdots + b_n s^n}, \tag{2}$$

where $N(s)$ denotes the numerator polynomial and $D(s)$ the denominator polynomial. After a discretization of (2), a simulation of the displacement $\hat{y}$ given a measured or simulated force input u at time step k is possible:

$$\begin{aligned}\hat{y}[k] = a_0 u[k] + \cdots + a_n u[k-n] \\ - b_1 \hat{y}[k-1] - \cdots - b_m \hat{y}[k-m].\end{aligned} \tag{3}$$

This mathematical description allows simulation across multiple transfer functions in the machine's working area by using the simulation results $\hat{y}$ of earlier functions as input for later functions. This is not possible, for example, when using a state space model to describe the system because of the non-unique representation of these models. This is because the states of multiple systems can vary in size due to the number of poles and, in addition, the physical meaning of the states is not the same across several systems. Therefore, it is not possible to transfer one system's final states as the next system's initial states. Instead, the states of the subsequent system would first have to be calculated from the results of the previous system in order to adopt the initial conditions and thus obtain a continuous simulation. However, this is more computationally intensive than using (3) in combination with transfer functions.

2. In the simplest application of `tfest`, only two inputs need to be specified: The data of the measured FRF as complex numbers and the number of poles of the system to be estimated. The number of zeros is automatically reduced by one compared to the number of poles [29]. In the present case, however, we reduce the number of zeros by three compared to the number of poles. The reason for this is that in industrial practice, vibration signals are often recorded with acceleration sensors. Thus, an accelerance is calculated as a result of the FRF measurement. However, since the LSRF method (implemented with the `tfest` command in Matlab) is designed to estimate transfer functions based on a receptance FRF, the accelerance FRF must be converted. This conversion is done by integrating the accelerance twice in the frequency domain. To do so, the accelerance FRF is multiplied by $(j\omega_i)^{-2}$. However, this procedure artificially creates two spurious poles in the receptance FRF. This is taken into account when estimating the transfer function. Two additional zeros are removed. Furthermore, it is possible to specify a frequency-dependent weighting filter $W(j\omega_i)$ (see (1)) as an additional input to `tfest`. The weighting filter can be used to apply additional influence to the function estimation.
3. The algorithm of the `tfest` command is highly performant and numerically stable at the same time [2]. This is due to the combination of the Sanathanan and Koerner iterations (SK) [24, 6], the frequency-domain instrumental variable iterations (IV) [12] and further mathematical methods such as domain mapping [22] and measurement scaling to avoid numerical problems and improve the conditioning number.

The following sections describe in more detail how `tfest` can be used and appropriately parameterized to estimate the transfer function.

3.1. Transfer function estimation considering a coherence threshold

In the publication by Oexle et al., the suitability of the LSRF method for mathematical modeling of FRFs was demonstrated using synthetic data obtained from simulation [19]. However, these synthetic data sets were completely noise-free. Real-world measured FRFs based on impact hammer measurements sometimes show significant noise, as can be seen in Figure 2 in the example of a measured FRF (green curve). The machine does not show a clear behavior in these frequency ranges. This is reflected in the coherence γ^2. The coherence is used to measure the reliability of the FRF's measured values [8]. It contains a value between 0 and 1 and is frequency-dependent. For $\gamma^2 \geq 0.8$, the associated FRF measurement values can be considered *usable* [10]. Accordingly, measurement values with a coherence $\gamma^2 < 0.8$ are defined as *unusable* because the machine does not provide a clear linear response at these frequencies. Thus, building a model based on transfer functions for these frequencies is not useful. Therefore, all measured values of a FRF with a respective $\gamma^2 < 0.8$ should be excluded from the transfer function estimation through the LSRF method. Accordingly, these are filtered out of the measurement data before the LSRF method is applied. However, this also means that the estimated transfer function should later only be used for a displacement simulation at the frequencies where $\gamma^2 \geq 0.8$ holds. If this is not observed, displacements may be simulated at frequencies where the estimated transfer function is not valid. Estimating the transfer function while considering $\gamma^2 \geq 0.8$ will result in the system behavior shown in Figure 2 as the blue curve. The gray-shaded frequency regions in the figure mark frequencies with $\gamma^2 < 0.8$ and thus are not included in the transfer function estimation. The number of poles used for the LSRF method was determined by an exhaustive search algorithm which samples poles from 4 to 60 and adopts the pole number of the estimated stable transfer function with the best fit between the green and blue curves. In addition, the FRF was already filtered with a 10-point centered moving average before transfer function estimation to remove small noise from the measured curve. When calculating the fit between the measured curve and the curve of the estimated transfer function, excluding the gray-shaded frequency ranges, the result is a fit of 81.46 %. In contrast to the FRAC

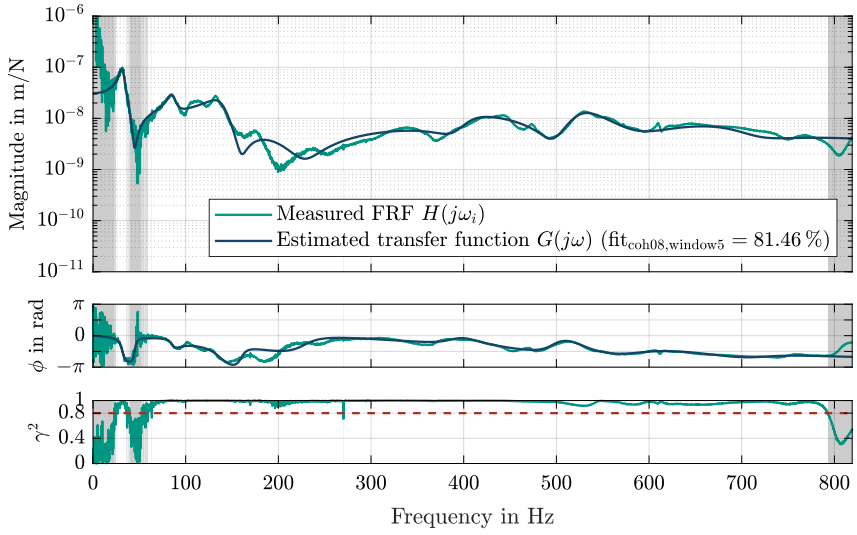

Figure 2. FRF of estimated transfer function (blue) based on measured FRF data (green). The frequencies where $\gamma^2 < 0.8$ are shaded gray and are not included in the calculation of the transfer function. Therefore, the same data is used to calculate the fit shown in the figure.

$$\text{FRAC} = \frac{|H^T G|^2}{(H^T H)(G^T G)} \tag{4}$$

introduced by Heylen and Lammens [13], which is often used for such comparisons, the normalized root mean squared error (NRMSE)

$$\text{fit} = \frac{\|H - G\|}{\|H - \text{mean}(H)\|} \tag{5}$$

is used here to calculate the fit value [27]. The advantage of a fit calculation with (5) instead of (4) is that (4) is insensitive to constant deviations in the amplitude and phase response [3]. Thus, (5) provides a more sensitive measure for comparing the FRF of the estimated transfer function with the measured FRF.

3.2. Coherence windowing

Looking more closely at the coherence in Figure 2, it is noticeable that the gray shaded areas sometimes contain narrow white lines. This is because the coherence value at these points exceeds the previously defined threshold of $\gamma^2 = 0.8$, which means that the measured values at these frequencies are considered *usable*. Accordingly, the FRF measurement values at these frequencies are included in the estimation of the transfer function. The algorithm of the LSRF method tries to fit the transfer function from the low-frequency poles to the higher-frequency poles. Accordingly, in this case, it will try to map measurement values in areas of the FRF that have high noise. This results in an error that makes it difficult, and sometimes impossible, to accurately map other frequencies (such as the frequencies between 150 Hz and 200 Hz in Figure 2). It also unnecessarily increases the order of the transfer function, making it more complex. To counteract this problems, two solutions can be adopted:

1. To avoid overfitting, the number of poles of an estimated transfer function can be included in the fit calculation [7].
2. Depending on the coherence, not only are measurement values of the FRF that have a coherence $\gamma^2 < 0.8$ not considered. Instead, each coherence value $\gamma^2 \geq 0.8$ must have neighbors within a given frequency window whose coherence is also $\gamma^2 \geq 0.8$. This ensures that coherence values $\gamma^2 \geq 0.8$ are valid.

Solution 1 avoids overfitting the FRF, but it is still not possible to control which frequency points are used to estimate the transfer function. In contrast, solution 2 cleans up the input data for the estimation. Accordingly, solution 2 is implemented in the next step. Here, the window size is set to 5 Hz, which, with a distance of 0.25 Hz between two data points in the measured FRF, results in a set of 20 neighboring frequency data points. This ensures, that only FRF values are used for the transfer function estimation whose corresponding coherence is consistently $\gamma^2 \geq 0.8$ over a frequency band of this given neighborhood. The result of the estimation is shown in Figure 3. The fit is improved from 81.46 % to 90.20 % compared to the result in Figure 2.

In addition, it can be clearly seen that the system behavior of the estimated transfer function (blue curve) fits very well to the measured FRF (green curve). In particular, the critical range

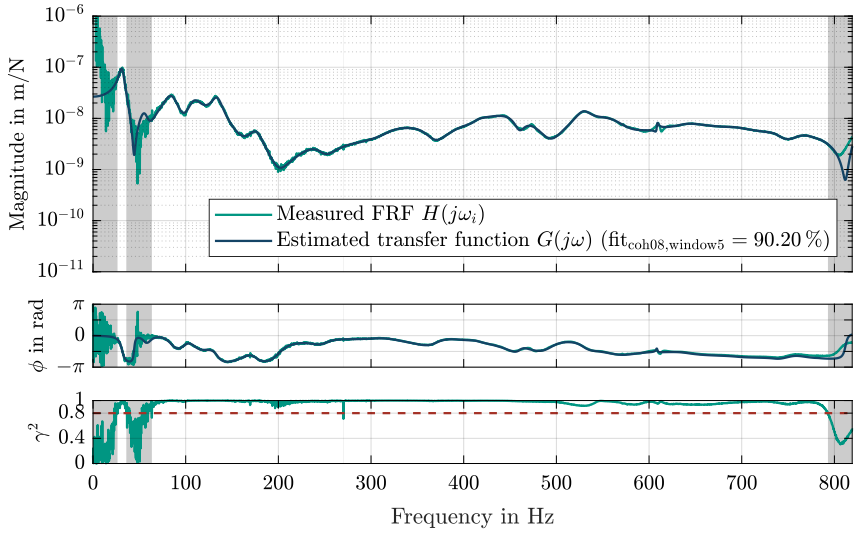

Figure 3. FRF of estimated transfer function (blue) based on measured FRF data (green). The frequencies at which the coherence of neighboring frequencies within a window of at least 5 Hz is $\gamma^2 < 0.8$ are shaded gray and are not included in the estimation of the transfer function. Therefore, the same data is used to calculate the fit shown in the figure.

between 150 Hz and 200 Hz in Figure 2 has improved significantly.

3.3. Transfer of the methodology to further measuring points in the machine's working area

In the previous chapters, it was shown in detail how the accuracy of the transfer function estimation using the LSRF method was significantly increased by pre-filtering the measurement data using the coherence γ^2. To test the procedure on other FRFs, a total of 162 FRFs were recorded within a DMC 60H. Over a X-travel of 640 mm and a Y-travel of 343.75 mm evenly distributed impact hammer measurements with force excitation were performed in the X, Y and Z directions and FRFs calculated. Subsequently, the transfer functions were estimated using the method described in Section 3.2. Figure 4 shows the number of transfer functions over the fit results for all measurements. The left histogram shows the fits where only all coherences $\gamma^2 < 0.8$ were removed prior to estimation (see Section 3.1). In contrast, the right histogram shows the fits with additional filtering with the 5 Hz window. Note that in both histograms, the fit values are calculated based on the coherence filtering with the 5 Hz windowing to allow a direct comparison of all values. Both the mean fit and the distribution of the fit results show that the pre-processing of the measurement data using the 5 Hz windowing has a positive influence on the fit of the estimated transfer functions. In addition, it can be seen that a fit of >70 % can be achieved for all 162 FRFs (histogram on the right). Figure 5 shows the result of the worst transfer function estimate of the right histogram with a fit of 73.14 %. It can be

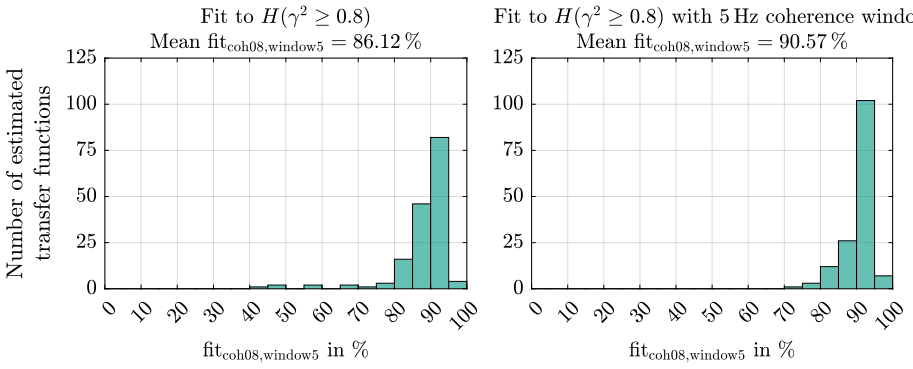

Figure 4. Frequency distribution of the fits of individual transfer function estimates. The left histogram shows the distribution based on all measured values with $\gamma^2 \geq 0.8$. On the right is the distribution based on the estimation of all data points for which all neighboring frequencies in a 5 Hz window have a coherence value of $\gamma^2 \geq 0.8$. The fits are calculated in both histograms using the 5 Hz windowing to be able to compare all values with each other.

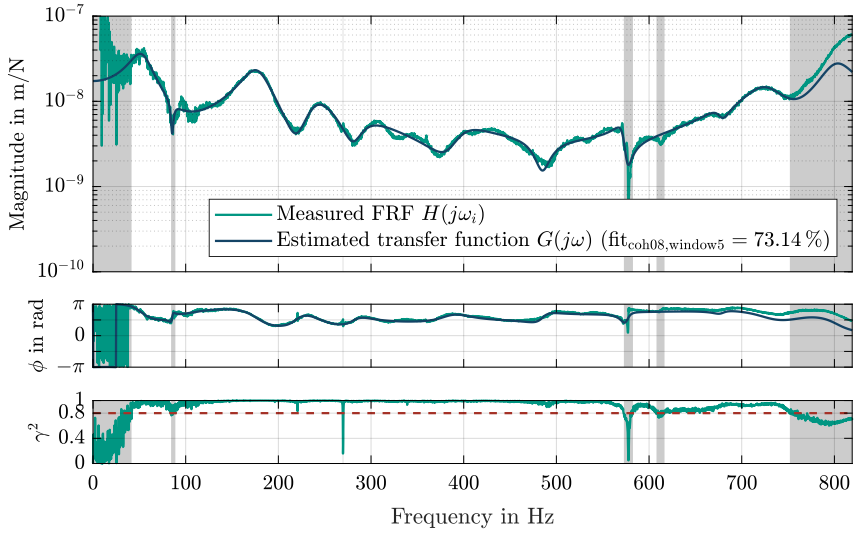

Figure 5. FRF of estimated transfer function (blue) based on measured FRF data (green) with the worst fit based on the values of the right histogram in Figure 4. The frequencies at which the coherence of neighboring frequencies within a window of at least 5 Hz is $\gamma^2 < 0.8$ are shaded gray and are not included in the calculation of the transfer function. Therefore, the same data is used to calculate the fit shown in the figure.

seen that the system behavior of the estimated transfer function (blue curve) and the measured FRF (green curve) match sufficiently well. Additionally, a residual analysis was performed for each estimated model to evaluate the mapping quality of every model. For all models, the magnitude of the residuals at most frequencies was found to be less than −20 dB. This result indicates a deviation of the model of less than 10 % with respect to the value of the measured FRF. Consequently, it can be concluded that a fit value >70 % can be used as a reliable indicator of model quality.

3.4. Use of the weighting filter

As mentioned in (1), the LSRF method can also be given a weighting filter W to influence the estimation of the transfer function. Depending on this, the different FRF measurements at different frequencies are taken into account differently in the cost function (1). The intuitive way of an adaptive weighting filter constructed by deriving the weighting filter from the difference between an already estimated transfer function and the measured FRF does not work. With such an implementation, the regions with the largest error receive a larger weight in a repeated estimation, but the regions with the smallest error receive only a small weight. Thus, repeated estimation will result in errors at this location. This cannot be avoided by adding or multiplying a constant factor to the weighting filter, as the LSRF algorithm normalizes the weighting error values internally. Instead, a weighting filter can be applied that amplifies small amplitudes in order to achieve a better balance between

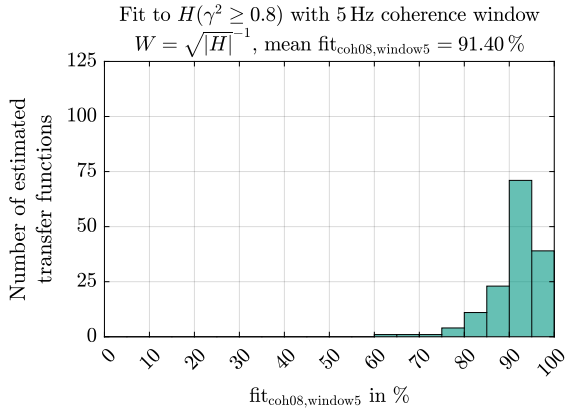

Figure 6. Frequency distribution of the fits of individual transfer function estimates using the weighting filter $W_{\text{invsqrt}} = \sqrt{|H|}^{-1}$.

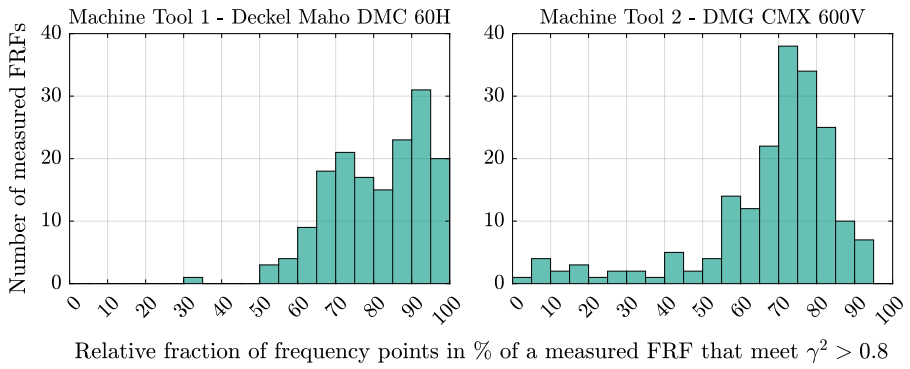

Figure 7. Quantitative analysis of the coherences of the measured FRFs. In this histogram, the relative fraction of the frequency points of the spectrum whose coherence is $\gamma^2 \geq 0.8$ is determined for each measured FRF. For machine tool 2 (DMG CMX 600V), 21 of the 189 measured FRFs have coherences in which not even 50 % of the frequency points fulfill the criterion $\gamma^2 \geq 0.8$. In contrast, machine tool 1 (Deckel Maho DMC 60H) only exhibits 1 out of the 162 measurements that do not fulfill $\gamma^2 \geq 0.8$.

large and small amplitudes in the calculation of (1). The weighting filter that is used for this purpose is described by

$$W_{\text{invsqrt}} = \frac{1}{\sqrt{|H(j\omega_i)|}} \tag{6}$$

[28]. Estimating all transfer functions from the right histogram in Figure 4 using this weighting filter, the result is shown in Figure 6. It can be seen that the mean fit of 91.40 % has increased slightly compared to the mean fit from the right histogram in Figure 4. In particular, the number of estimated transfer functions with a fit between 95 % and 100 % is larger. However, there are also two transfer functions that only have a fit between 60 % and 70 %. These are below the 70 % limit mentioned above. In summary, the use of the weighting filter W_{invsqrt} has a positive influence on the fits of the individual transfer functions. However, some transfer functions estimated with a lower fit should be reestimated without the weighting filter W_{invsqrt} and then used.

3.5. Validation on measured compliance frequency response functions with poor coherence

After the previous sections have shown how the LSRF method enables a good mapping accuracy of the measurement data by suitable pre-filtering of the measurement data depending on the coherence and the setting of a suitable weighting filter, the method is tested on FRFs of another machine (DMG CMX 600V). However, as illustrated in Figure 7, in contrast to the previous measurements, a significantly poor coherence was achieved for the individual FRFs. Consequently, windowing with a window size of 5 Hz (see Section 3.2) means that a larger part of the frequencies is not considered in the estimation of the transfer function. The results of the estimation over all FRFs are shown in Figure 8. The left side shows the distribution of the fits without the use of any specific weighting filter, while the results of the right histogram were calculated using the weighting filter W_{invsqrt}. Again, as in Section 3.4, there is

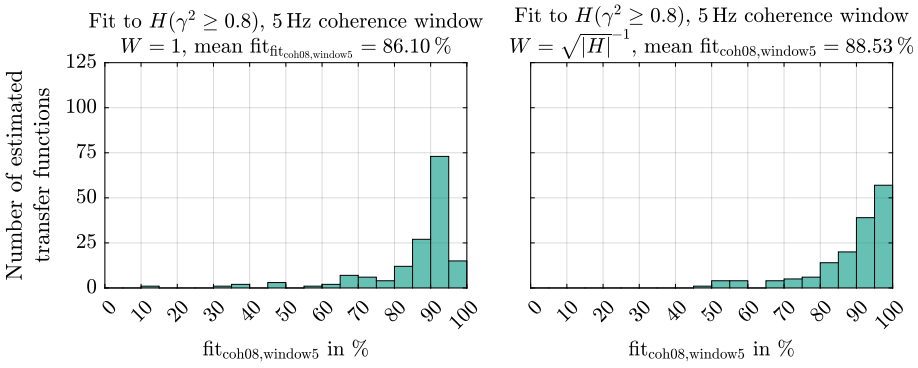

Figure 8. Results of transfer function estimation using measured FRFs on a different machine tool with poor coherence. In the left histogram, the estimation is performed without a specific weighting filter. In the right histogram, the weighting filter $W_{\text{invsqrt}} = \sqrt{|H|}^{-1}$ is used. The fits are calculated in both histograms using the 5 Hz windowing to be able to compare all values with each other.

a clear improvement in the fit values using the weighting filter W_{invsqrt}. Nevertheless, a total number of 13 transfer functions can be identified with a fit of less than 70 %. Seven of them are located in the area above 70 % in the left histogram, which means that a better fit can be achieved for them without the use of a specific weighting filter, as already described in Section 3.4. However, the remaining six transfer functions cannot be improved by this procedure either. This shows the limitations of the presented method: consistently good fit results cannot be guaranteed for measurement data with poor coherence.

4. Conclusion and Outlook

In view of a future automated method for the generation of machine dynamic models of milling machines [19], this paper presents a method with which transfer functions can be estimated with a large fit compared to measured FRFs using the LSRF method proposed by Arda Ozdemir and Gumussoy [2]. Contrary to many state-of-the-art publications, the coherence of the measurements is used to pre-filter the measurement data. In addition, a weighting filter is used to influence the weighting of individual frequencies within the transfer function estimation. Measurement data within the FRFs with a low amplitude value are weighted higher to balance their influence on the cost function used by the LSRF algorithm with the influence of large amplitude values. Using this procedure, fits >70 % between the measured data and the estimated transfer function can be consistently achieved for measured FRFs with good coherence. For FRFs with poor coherence, this goal can also be achieved for most transfer functions, although it is difficult to guarantee. In future work, further combinations of the weighting filter can be investigated to increase the accuracy of the fits on FRFs with poor coherence. However, the primary goal should always be to obtain measurements with good coherence. Furthermore, the magnitudes of the residuals from the residual analyses performed could be used to define the validity ranges of the estimated transfer functions across frequencies for a subsequent application within a simulation.

Author Contribution

Conceptualization, F.O. and F.H.; methodology, F.O. and F.H.; software, F.O. and F.H.; validation, F.O. and F.H.; formal analysis, F.O. and F.H.; investigation, F.O. and F.H.; resources, A.P. and J.F.; data curation, F.O. and F.H.; writing—original draft preparation, F.O.; writing—review and editing, F.H., F.O., A.P. and J.F.; visualization, F.H.; supervision, A.P. and J.F.; project administration, F.O. and J.F.

References

[1] Altintas, Y., 2012. Manufacturing automation: metal cutting mechanics, machine tool vibrations, and CNC design. 2nd ed., Cambridge university press, Cambridge.

[2] Arda Ozdemir, A., Gumussoy, S., 2017. Transfer Function Estimation in System Identification Toolbox via Vector Fitting. IFAC-PapersOnLine 50, 6232–6237. URL: https://linkinghub.elsevier.com/retrieve/pii/S2405896317315045, doi:10.1016/j.ifacol.2017.08.1026.

[3] Babuska, V., Carter, D., Lane, S., Lacy, S., 2005. FRF Correlation and Error Metrics for Plant Identification, in: 46th AIAA/ASME/ASCE/AHS/ASC Structures, Structural Dynamics and Materials Conference. American Institute of Aeronautics and Astronautics. Structures, Structural Dynamics, and Materials and Co-located Conferences. URL: https://arc.aiaa.org/doi/10.2514/6.2005-2012, doi:10.2514/6.2005-2012.

[4] Bergs, T., Biermann, D., Erkorkmaz, K., M'Saoubi, R., 2023. Digital twins for cutting processes. CIRP Annals 72, 541–567. URL: https://linkinghub.elsevier.com/retrieve/pii/S000785062300135X, doi:10.1016/j.cirp.2023.05.006.

[5] Bergs, T., Gierlings, S., Auerbach, T., Klink, A., Schraknepper, D., Augspurger, T., 2021. The Concept of Digital Twin and Digital Shadow in Manufacturing. Procedia CIRP 101, 81–84. URL: https://linkinghub.elsevier.com/retrieve/pii/S2212827121006612, doi:10.1016/j.procir.2021.02.010.

[6] Drmač, Z., Gugercin, S., Beattie, C., 2015. Quadrature-Based Vector Fitting for Discretized $\mathcal{H}_2$ Approximation. SIAM Journal on Scientific Computing 37, A625–A652. URL: http://epubs.siam.org/doi/10.1137/140961511, doi:10.1137/140961511.

[7] Ellinger, J., Beck, L., Benker, M., Hartl, R., Zaeh, M.F., 2023. Automation of Experimental Modal Analysis Using Bayesian Optimization. Applied Sciences 13, 949. URL: https://www.mdpi.com/2076-3417/13/2/949, doi:10.3390/app13020949.

[8] Ewins, D.J., 2000. Modal testing: theory, practice and application. Number 10 in Mechanical engineering research studies engineering dynamics series. 2nd ed., Research Studies Press, Baldock.

[9] FTI Consulting, Inc., 2020. STEM and the American Workforce , 46URL: https://www.fticonsulting.com/~/media/Files/us-files/insights/reports/2020/march/stem-american-workforce.pdf.

[10] Goldman, S., 1991. Vibration spectrum analysis : a practical approach. 1st ed., Industrial Press Inc., New York.

[11] Guillaume, P., Verboven, P., Vanlanduit, S., Van der Auweraer, H., Peeters, B., 2003. A poly-reference implementation of the least-squares complex frequency-domain estimator. Proceedings of IMAC 21.

[12] van Herpen, R., Oomen, T., Steinbuch, M., 2014. Optimally conditioned instrumental variable approach for frequency-domain system identification. Automatica 50, 2281–2293. URL: https://www.sciencedirect.com/science/article/pii/S0005109814002775, doi:10.1016/j.automatica.2014.07.002. number: 9.

[13] Heylen, W., Avitabile, P., 1998. Correlation Considerations – Pt. 5 (Degree of Freedom Correlation Techniques). Proceedings of the 16th International Modal Analysis Conference (IMAC) , 207–214.

[14] Kipfmüller, M., 2010. Aufwandsoptimierte Simulation von Werkzeugmaschinen. URL: https://publikationen.bibliothek.kit.edu/1000014668, doi:10.5445/IR/1000014668. iSBN: 9783832287641 ISSN: 0724-4967.

[15] Lau, J., Lanslots, J., Peeters, B., Van der Auweraer, H., 2007. Automatic Modal Analysis – Myth or Reality?, in: Proceedings of the 25th International Modal Analysis Conference, Orlando, Fl, USA.

[16] Markatos, N.G., Mousavi, A., 2023. Manufacturing quality assessment in the industry 4.0 era: a review. Total Quality Management & Business Excellence 34, 1655–1681. URL: https://www.tandfonline.com/doi/full/10.1080/14783363.2023.2194524, doi:10.1080/14783363.2023.2194524.

[17] Mugnaini, V., Zanotti Fragonara, L., Civera, M., 2022. A machine learning approach for automatic operational modal analysis. Mechanical Systems and Signal Processing 170, 108813. URL: https://linkinghub.elsevier.com/retrieve/pii/S0888327022000127, doi:10.1016/j.ymssp.2022.108813.

[18] Neu, E., Janser, F., Khatibi, A.A., Orifici, A.C., 2017. Fully Automated Operational Modal Analysis using multi-stage clustering. Mechanical Systems and Signal Processing 84, 308–323. URL: https://linkinghub.elsevier.com/retrieve/pii/S0888327016302552, doi:10.1016/j.ymssp.2016.07.031.

[19] Oexle, F., Heimberger, F., Puchta, A., Fleischer, J., 2024. Concept for Individual and Lifetime-Adaptive Modeling of the Dynamic Behavior of

Machine Tools. Machines 12, 123. URL: https://www.mdpi.com/2075-1702/12/2/123, doi:10.3390/machines12020123.

[20] Peeters, B., Van Der Auweraer, H., Guillaume, P., Leuridan, J., 2004. The PolyMAX Frequency-Domain Method: A New Standard for Modal Parameter Estimation? Shock and Vibration 11, 395–409. URL: https://onlinelibrary.wiley.com/doi/10.1155/2004/523692, doi:10.1155/2004/523692.

[21] Peichl, A., Sauer, S., Wohlrabe, K., 2022. Fachkräftemangel in Deutschland und Europa – Historie, Status quo und was getan werden muss. ifo Schnelldienst 75, 70–75. URL: https://www.ifo.de/en/publications/2022/article-journal/fachkraeftemangel-deutschland-und-europa-historie-status-quo.

[22] Pintelon, R., Schoukens, J., 2012. System identification: a frequency domain approach. 2. ed., Wiley IEEE Press, Hoboken, N.J. Piscataway, NJ.

[23] Reynders, E., Houbrechts, J., De Roeck, G., 2012. Fully automated (operational) modal analysis. Mechanical Systems and Signal Processing 29, 228–250. URL: https://linkinghub.elsevier.com/retrieve/pii/S0888327012000088, doi:10.1016/j.ymssp.2012.01.007.

[24] Sanathanan, C., Koerner, J., 1963. Transfer function synthesis as a ratio of two complex polynomials. IEEE Transactions on Automatic Control 8, 56–58. URL: https://ieeexplore.ieee.org/document/1105517?reload=true&arnumber=1105517, doi:10.1109/TAC.1963.1105517. number: 1 Conference Name: IEEE Transactions on Automatic Control.

[25] Scionti, M., Lanslots, J., 2005. Stabilisation diagrams: Pole identification using fuzzy clustering techniques. Advances in Engineering Software 36, 768–779. URL: https://linkinghub.elsevier.com/retrieve/pii/S0965997805001250, doi:10.1016/j.advengsoft.2005.03.029.

[26] Scionti, M., Lanslots, J., Goethals, I., Vecchio, A., Peeters, B., Moor, B.D., 2003. Tools to Improve Detection of Structural Changes from In-Flight Flutter Data URL: https://api.semanticscholar.org/CorpusID:59812988.

[27] The MathWorks Inc., 2024a. Compare identified model output with measured output - MATLAB compare - MathWorks Deutschland. URL: https://de.mathworks.com/help/ident/ref/compare.html. abgerufen am 09.02.2024.

[28] The MathWorks Inc., 2024b. Option set for tfest - MATLAB - MathWorks Deutschland. URL: https://de.mathworks.com/help/ident/ref/tfestoptions.html. abgerufen am 07.02.2024.

[29] The MathWorks, Inc., 2024. tfest - Estimate transfer function model - MATLAB - MathWorks Deutschland. URL: https://de.mathworks.com/help/ident/ref/tfest.html.

[30] Van Overschee, P., De Moor, B., 1996. Subspace Identification for Linear Systems. Springer US, Boston, MA. URL: http://link.springer.com/10.1007/978-1-4613-0465-4, doi:10.1007/978-1-4613-0465-4.

[31] Verboven, P., 2002. Frequency Domain System Identification for Modal Analysis. PhD Thesis. Brussels.

[32] Vold, H., Kundrat, J., Rocklin, G.T., Russell, R., 1982. A Multi-Input Modal Estimation Algorithm for Mini-Computers, SAE Transactions. pp. 815–821. URL: https://www.sae.org/content/820194/, doi:10.4271/820194.

[33] Weck, M., Brecher, C., 2013. Werkzeugmaschinen. 5: Messtechnische Untersuchung und Beurteilung, dynamische Stabilität. 7th ed., Springer Vieweg, Berlin Heidelberg.

[34] Westkämper, E., Löffler, C., 2016. Strategien der Produktion: Technologien, Konzepte und Wege in die Praxis. 1st ed., Springer Berlin Heidelberg, Berlin, Heidelberg. URL: http://link.springer.com/10.1007/978-3-662-48914-7, doi:10.1007/978-3-662-48914-7.